Solar Cells

Deutsche Ausgabe: DOI: 10.1002/ange.201602097
Internationale Ausgabe: DOI: 10.1002/anie.201602097

A Graphene Composite Material with Single Cobalt Active Sites: A Highly Efficient Counter Electrode for Dye-Sensitized Solar Cells

Xiaoju Cui[+], Jianping Xiao[+], Yihui Wu, Peipei Du, Rui Si, Huaixin Yang, Huanfang Tian, Jianqi Li, Wen-Hua Zhang, Dehui Deng,* and Xinhe Bao*

Abstract: *The design of catalysts that are both highly active and stable is always challenging. Herein, we report that the incorporation of single metal active sites attached to the nitrogen atoms in the basal plane of graphene leads to composite materials with superior activity and stability when used as counter electrodes in dye-sensitized solar cells (DSSCs). A series of composite materials based on different metals (Mn, Fe, Co, Ni, and Cu) were synthesized and characterized. Electrochemical measurements revealed that CoN_4/GN is a highly active and stable counter electrode for the interconversion of the redox couple I^-/I_3^-. DFT calculations revealed that the superior properties of CoN_4/GN are due to the appropriate adsorption energy of iodine on the confined Co sites, leading to a good balance between adsorption and desorption processes. Its superior electrochemical performance was further confirmed by fabricating DSSCs with CoN_4/GN electrodes, which displayed a better power conversion efficiency than the Pt counterpart.*

Dye-sensitized solar cells (DSSCs) consist of three important components, a photoactive working electrode (WE), a counter electrode (CE), and a redox-active electrolyte,[1] and they are relatively simple, practical, and economical photovoltaic devices for the efficient conversion of solar energy into electricity.[2] The CE is a crucial component governing the catalytic reduction of redox couples and the power conversion efficiency.[3] An excellent CE should exhibit high electrical conductivity, high electrocatalytic activity for the regeneration of the redox couples, and long-term stability in the working electrolyte. At present, platinum is widely utilized as a standard CE owing to its excellent electrocatalytic activity, stability, and device efficiency in DSSCs. However, platinum is extremely rare and expensive, which prevents its use in the large-scale commercialization of DSSCs. Recent studies have demonstrated that an optimization of the CE can significantly improve the overall efficiency of DSSCs.[4] Therefore, searching for alternative CEs that are based on abundant and inexpensive elements has become an important topic to enable the large-scale commercialization of DSSCs.[5]

Graphene has been shown to possess high chemical stability and electrical conductivity.[6] The functionalization of graphene is considered to be an efficient approach to develop efficient CEs for DSSCs.[7] It has been found that single Fe active sites, with the active Fe atoms anchored by nitrogen atoms in the interstices of the graphitic sheets, can significantly improve the catalytic activity of graphene in the oxygen reduction reaction (ORR).[8] Recently, density functional theory (DFT) calculations have confirmed the ORR activity of single Fe active sites confined within graphene.[9] However, it is still unclear whether functionalized graphene is sufficiently active and stable to be used as an alternative CE material for DSSCs. In our previous work,[10] we developed a practical approach to incorporate single Fe sites into graphene nanosheets. The catalytic activity of various 3d transition metals (Mn, Fe, Co, Ni, and Cu) confined within graphene in DSSCs can thus be investigated.

Herein, we first prepared a series of composite materials with confined MN_4 (M = Mn, Fe, Co, Ni, or Cu) moieties in the basal plane of graphene nanosheets (MN_4/GN) by a well-tested procedure.[10] In brief, the MN_4/GN composites were prepared by ball milling of a metal phthalocyanine and graphene nanosheets under suitable conditions. The corresponding metal phthalocyanine precursors and synthesized composites are abbreviated as MPc and MN_4/GN (M = Mn, Fe, Co, Ni, or Cu), respectively. A representative image of CoN_4/GN obtained by high-angle annular dark field scanning transmission electron microscopy (HAADF-STEM) with sub-Ångström resolution is shown in Figure 1 a. Well-dispersed white dots (highlighted by black circles) were observed within the graphene nanosheets (GN), and could be attributed to Co atoms, whose atomic number is larger than that of C and N. Furthermore, Raman spectroscopy (Supporting Information, Figure S1 a) and X-ray diffraction (XRD; Figure S1 b) indicate that the crystalline structure of

[*] X. Cui,[+] Dr. J. Xiao,[+] Prof. D. Deng, Prof. X. Bao
State Key Laboratory of Catalysis
Collaborative Innovation Center of Chemistry for Energy Materials
Dalian Institute of Chemical Physics
Chinese Academy of Sciences
Zhongshan Road 457, Dalian 116023 (China)
E-mail: dhdeng@dicp.ac.cn
Dr. Y. Wu, Prof. W.-H. Zhang
Sichuan Research Center of New Materials
Institute of Chemical Materials
China Academy of Engineering Physics
596 Yinhe Road, Shuangliu, Chengdu 610200 (China)
E-mail: whzhang@caep.cn
P. Du, Prof. R. Si
Shanghai Synchrotron Radiation Facility
Shanghai Institute of Applied Physics
Chinese Academy of Sciences, Shanghai 201204 (China)
Prof. H. Yang, Prof. H. Tian, Prof. J. Li
Beijing National Laboratory for Condensed Matter Physics
Institute of Physics, Chinese Academy of Sciences
Beijing 100190 (China)
[+] These authors contributed equally to this work.

Supporting information for this article can be found under: http://dx.doi.org/10.1002/anie.201602097.

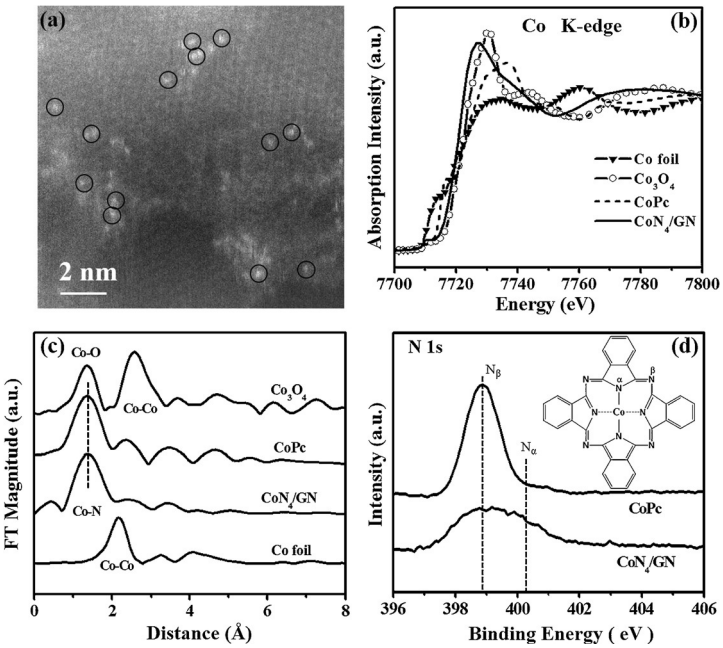

Figure 1. Morphology and structural characterization of CoN_4/GN samples. a) HAADF-STEM image of CoN_4/GN. b) Co K-XANES and c) Fourier-transformed EXAFS spectra of CoN_4/GN and CoPc, Co foil, and Co_3O_4 (not phase-shift-corrected). d) N 1s XPS spectra of CoN_4/GN and CoPc.

CoPc is lost when the CoN_x species are incorporated into GN through ball milling (see Figure S1 for more details).

X-ray absorption near-edge structure (XANES), extended X-ray absorption fine structure (EXAFS), and XPS analysis were further used to determine the chemical state and coordination of the Co atoms in CoN_4/GN. As shown in Figure 1b, a XANES spectroscopic signature corresponding to a planar CoN_4 geometry was observed at approximately 7716 eV in the Co K edge spectrum of a CoPc sample, whereas it was not observed for CoN_4/GN samples, indicating that the square-planar configuration of the active CoN_4 sites may be modified by hydroxy groups upon exposure to air after ball milling. Further Fourier-transformed EXAFS spectra in Figure 1c show that the Co/N coordination structure in CoN_4/GN is the same as in the CoPc sample without forming Co–Co scattering paths. Thus the XAS spectra clearly reveal that the local CoN_4 structure is retained. Furthermore, the N 1s XPS spectrum (Figure 1d) of CoN_4/GN shows that the intensity ratio of pyridinic N_β (398.8 eV; attached to a carbon atom of the outer macrocycle) to pyrrolic N_α (400.3 eV; attached to Co) is significantly reduced with respect to CoPc, indicating that the pyridinic N_β species have been destroyed by ball milling while pyrrolic N_α species are still found in CoN_4/GN. Therefore, the single Co sites are likely to be bonded to four neighboring pyrrolic N_α atoms and embedded in the basal plane of graphene. This is consistent with our previous finding for FeN_4/GN.[10] Detailed XRD, Raman spectroscopy, and XPS data for other MN_4/GN (M = Mn, Fe, Ni, and Cu) composites are given in the Supporting Information (Figures S3–S10).

Moreover, we also calculated the stability of all MN_x/GN (M = Mn, Fe, Co, Ni, or Cu; $x = 1, 2, 3,$ and 4) materials by comparing the formation energies, E_f [Eq. (1)]:

$$E_f = E_{tot} - n_C\mu_C - n_N\mu_N - n_M\mu_M \quad (1)$$

where E_{tot} is the total energy from the DFT calculations, n_C, n_N, and n_M are the number of carbon, nitrogen, and metal atoms in the studied structures, respectively, and μ_C, μ_N, μ_M are the chemical potentials of carbon, nitrogen, and metal atoms relative to graphene, a nitrogen molecule, and single metal atoms, respectively. As shown in Table S1, the MN_4/GN (M = Mn, Fe, Co, Ni, or Cu) compounds are more stable than the other MN_x/GN ($x = 1$, 2, and 3) structures.

The electrocatalytic activity of CEs based on these materials was assessed by cyclic voltammetry measurements. In Figure 2a, two pairs of oxidation and reduction peaks [Ox-1/Red-1 (left) and Ox-2/Red-2 (right)] are well-resolved for all of the studied electrodes, which can be attributed to the oxidation and reduction reactions of I^-/I_3^- and I_3^-/I_2, respectively. Herein, we only focus on the redox pair I^-/I_3^- on the left (IRR = triiodide reduction reaction, Ox-1 and Red-1).

The peak current density and the peak separation between the anodic and cathodic peaks (Epp) are useful parameters for evaluating the catalytic activity of CEs. The reaction rate of the IRR positively correlates with the peak current density, while it negatively correlates with Epp. As shown in Figure 2a, the CE based on CoN_4/GN exhibited the best performance and gave an Epp value of 135 mV, which is much smaller than the Epp value of 215 mV achieved with a sputtered Pt electrode. Furthermore, the Epp values of all studied MN_4/GN CEs follow the order of MnN_4/GN > FeN_4/GN > CoN_4/GN < NiN_4/GN < CuN_4/GN. Moreover, the peak current densities decreased exactly in reversed order, MnN_4/GN < FeN_4/GN < CoN_4/GN > NiN_4/GN > CuN_4/GN. The CoN_4/GN CE exhibited a significantly higher peak current density than the other CEs, indicating that the CoN_4/GN CE has an outstanding electrochemical activity for the IRR, which is even superior to that of Pt electrodes.

Electrochemical impedance spectroscopy (EIS) is another useful approach to elucidate the electrocatalytic IRR activity of different CEs because it reflects the characteristics of the intrinsic interfacial charge transfer and charge transport kinetics at the electrode/electrolyte interface. Therefore, we further investigated the effects of introducing various MN_4 into graphene by EIS by using symmetric cells fabricated from two identical CEs. The Nyquist plots obtained from symmetric cells with different CEs are shown in Figure 2c. The semicircles in the high-frequency range indicate the charge transfer resistance (R_{ct}) at the electrode/electrolyte interface for the IRR, which varies inversely with the IRR activity of the CE. The semicircles in the low-frequency range represent the Nernst diffusion impedance (Z_N) of the redox couples in the electrolyte. The Nyquist plots were fitted by the Z-view

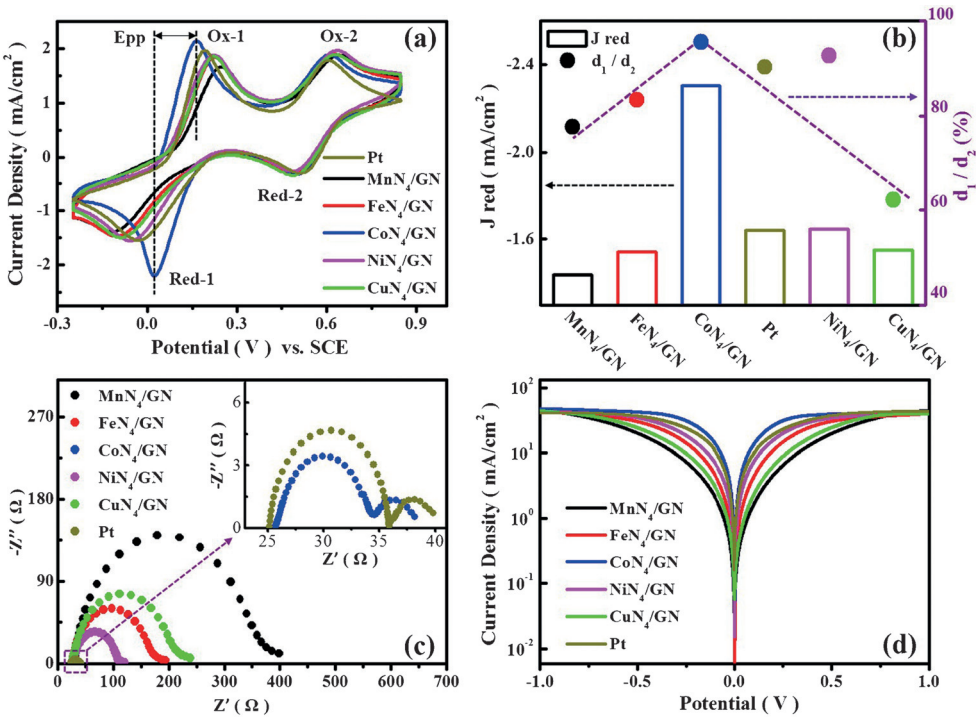

Figure 2. IRR performance of MN_4/GN composites (M = Mn, Fe, Co, Ni, or Cu) and a standard Pt electrode. a) Cyclic voltammograms. b) Reduction current density for the IRR in symmetric cells, and CE durability tests based on the d_1/d_2 ratio of the semicircle diameters before and after scanning 10 cycles of impedance spectra in Figure S12. c) Electrochemical impedance spectra. d) Tafel polarization curves of symmetric cells.

software with an equivalent circuit diagram, and the corresponding EIS parameters are shown in Table S3. The EIS results reveal that the catalytic activities decrease in the order of CuN_4/GN < NiN_4/GN < CoN_4/GN > Pt > FeN_4/GN > MnN_4/GN, which is consistent with the CV data. It has been reported that the diffusion coefficient of triiodide in DSSCs increases with increasing electrocatalytic activity of the CE whereas it shows an inverse correlation with Z_N. Smaller R_{ct} values imply lower internal resistance and higher catalytic activity of a CE, which is favorable for enhancing the device performance. Moreover, Tafel polarization was employed to scrutinize the catalytic activity of all CEs. The slopes of the anodic and cathodic traces at the Tafel zone again reveal that CoN_4/GN is the best CE material compared with other MN_4/GN and Pt electrodes (Figure 2d). All in all, the electrochemical characterization indicates the CoN_4/GN could be used as an alternative CE.

Furthermore, it is indispensable to understand the electrochemical stability of highly active CEs before they can be applied in DSSCs. Hence, we analyzed the changes in the impedance spectra for MN_4/GN- and Pt-based symmetric cells by subjecting them to ten sequential EIS scans. The variation in R_{ct} is negligible for CoN_4/GN, whereas it increased slightly for the Pt electrode after ten cycles. Therefore, the CoN_4/GN material also shows better electrochemical stability in DSSCs than Pt electrodes (Figure S12). Furthermore, the ratio d_1/d_2 of the semicircle diameters before and after ten cycles of impedance spectroscopy was employed to evaluate the durability of the counter electrode based on MN_4/GN. It is interesting that CoN_4/GN was located in the volcano curve maximum (Figure 2b), demonstrating its excellent stability. These results again show the advantages of CoN_4/GN-based CEs for DSSCs.

Moreover, we examined the electrochemical performance of all MN_4/GN samples by DFT calculations. The electrochemical performance of a CE is tightly correlated with its activity for IRR, where the IRR can be generally described as follows:

$$I_3^-(sol) \leftrightarrow I_2(sol) + I^-(sol) \quad (2)$$

$$I_2(sol) + 2^* \rightarrow 2I^* \quad (3)$$

$$I^* + e^- \rightarrow I^-(sol) \quad (4)$$

where * represents the free active sites on a CE material, and (sol) denotes the acetonitrile solution. Eq. (2) has been shown to be in fast equilibrium.[11] In contrast, I_2 dissociation and the desorption of adsorbed I atoms determine the overall electrocatalytic IRR activity of CE materials. According to the classical Brønsted–Evans–Polanyi relation,[12] the optimal IRR activity requires an intermediate I atom adsorption energy ($E_{ad,I}$).

We first examined the intrinsic activity of CoN_4/GN in the IRR and the energy profile along the reaction pathway in the absence of solvent effects and electrode voltage. As shown in Figure 3, an I_2 molecule and an I atom can preferably bind to an active Co center with the same adsorption energy of −0.72 eV. In other words, I_2 dissociation does not limit the overall IRR reaction rate. In contrast, from a thermodynamic point of view, the desorption of an I atom is rather difficult (1.43 eV). In the case of charged CoN_4/GN, the energetic trends shown in parentheses in Figure 3 are completely consistent with the above analyses. I_2 dissociation is sponta-

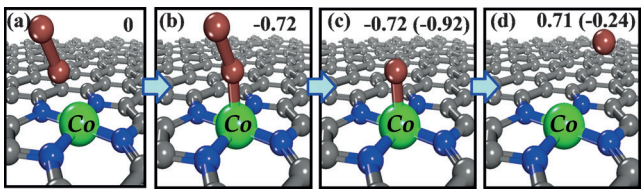

Figure 3. Calculated energies of intermediates of the IRR. a) Bare CoN_4/GN and an I_2 molecule, b) adsorbed I_2 molecule, c) adsorbed I atom, and d) desorbed I atom, along the reaction pathway of I_2 reduction (in eV), relative to the bare CoN_4/GN and I_2 molecule shown in (a). Negative reaction energies indicate thermodynamically favorable processes.

neous (−0.92 eV) and the rate-limiting step as the desorption of an I anion requires approximately 0.70 eV.

Then, we calculated the binding energies of iodine, $E_{ad,I}$, with the active centers of a series of MN_4/GN derivatives (M = Mn, Fe, Co, Ni, and Cu). The established kinetic model (see the Supporting Information) predicts the optimal $E_{ad,I}$ for the IRR to be about −0.80 eV, corresponding to that on the CoN_4/GN structure (Figure 4b). This is also consistent with earlier predictions,[13] where the optimal $E_{ad,I}$ was proposed to be in the range of −0.33 to −1.20 eV. The $E_{ad,I}$ on a Pt electrode, however, is only approximately 0.50 eV,[13] corresponding to non-optimal activity owing to the limited number of adsorbed iodine anions. For comparison, the $E_{ad,I}$ on CoN_4/GN is −0.80 eV.

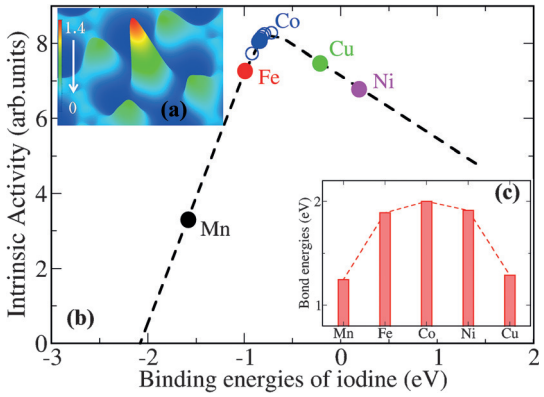

Figure 4. Calculated intrinsic activity and stability of MN_4/GN (M = Mn, Fe, Co, Ni, or Cu). a) Isosurface of the charge density at the active site for CoN_4/GN (e a.u.$^{-3}$). b) The intrinsic activity of MN_4/GN regarding the IRR on the CE is denoted by filled circles; the open circles correspond to CoN_4/GN taking solvent effects and charged states into account. c) The stability of MN_4/GN structures in terms of the M–N bond energies.

Furthermore, we examined the variation in $E_{ad,I}$ in combination with charging and solvent effects, as shown in Figure 4b by the open circles and blue points. Surprisingly, all $E_{ad,I}$ values are close to the maximum of the volcano plot (−0.80 eV). In other words, single Co sites attached to four N atoms in graphene are likely to have sustainable activity in electrocatalytic processes, and can outcompete a standard Pt electrode. Furthermore, the confined CoN_4 structures have the highest stability of all of these MN_4/GN structures (Figure 4c), which can be attributed to the highest stability of Co–N bonds in comparison with other metals. The stabilities of other MN_4/GN structures are further discussed in the Supporting Information (Figure S12).

The excellent electrochemical performance of the CE made of CoN_4/GN can be attributed to the synergy between stability and intrinsic activity. As the single Co active sites are confined in the basal plane of graphene, the moderate Co–N bond length constitutes only a minimal mismatch compared with other elements. Meanwhile, the moderate binding strength between Co and I leads to the high efficiency for I_2 dissociation and the desorption of I anions. Both the theoretical results and experimental measurements demonstrate these features of CoN_4/GN. From a theoretical point of view, the activity of CEs can be improved by circumventing the linear scaling relation,[12,13] that is, by stabilizing transition states instead of strengthening the adsorption energies of reactants.

Finally, we fabricated solar cell devices by using these MN_4/GN (M = Mn, Fe, Co, Ni, and Cu) composites as CEs of DSSCs to examine the device performance. The current density–voltage (*J*–*V*) curves and the corresponding photovoltaic parameters are presented in Figure 5 and Table S4,

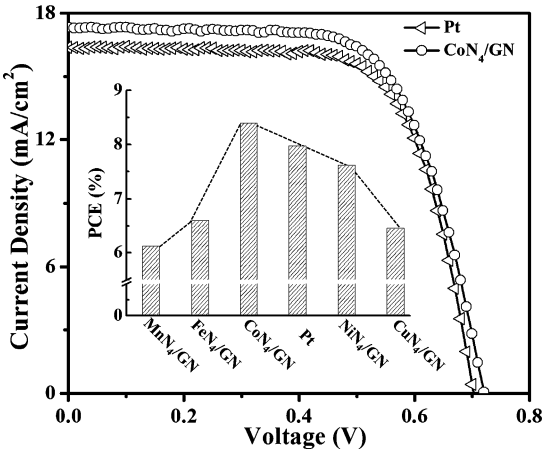

Figure 5. *J*–*V* curves for DSSCs made from CoN_4/GN and Pt. Inset: Measured PCEs of DSSCs fabricated with CEs made from different MN_4/GN and Pt.

respectively. Obviously, these devices show power conversion efficiencies (PCEs) in the order of MnN_4/GN < FeN_4/GN < CoN_4/GN > NiN_4/GN > CuN_4/GN. Moreover, the device made from the CoN_4/GN CE gave the best performance, which is reasonably in line with our electrochemical characterizations and DFT calculations. It is notable that compared to the control Pt-based device, the CoN_4/GN-based device exhibited a comparable FF and better J_{sc} and V_{oc} values, consequently yielding a superior device efficiency (8.40%) compared to the Pt counterpart (7.98%). Therefore, aside from being made from abundant elements and the feasible synthesis, CoN_4/GN composites combine the advantages of high electrocatalytic activity, excellent electrochemical stability, and superior device performance, rendering it an ideal CE for DSSCs.

In conclusion, a series of MN_4/GN (M = Mn, Fe, Co, Ni, or Cu) composites have been synthesized and characterized by high-resolution transmission electron microscopy, X-ray absorption spectroscopy, X-ray photoelectron spectroscopy, and Raman spectroscopy. Electrochemical characterization showed that a CE made of CoN_4/GN benefits from impressive stability and activity. DFT calculations confirmed that single Co active sites confined to the basal plane of graphene indeed possess excellent stability and intrinsic activity towards triiodide reduction. Furthermore, dye-sensitized solar cells were fabricated based on a variety of MN_4/GN composites. The DSSC device made of CoN_4/GN shows high electrocatalytic activity, excellently electrochemical stability, and

superior performance compared with conventional Pt electrodes, demonstrating its great potential.

Acknowledgements

We gratefully acknowledge financial support from the National Natural Science Foundation of China (21321002, 21573220, and 21303191), the Strategic Priority Research Program of the Chinese Academy of Sciences (XDA09030100), the China Postdoctoral Science Foundation (2014M551131), and the Outstanding Postdoctoral Award DMTO Project from the Dalian Institute of Chemical Physics, Chinese Academy of Sciences. We also thank the staff of the BL14W1 beamline at the Shanghai Synchrotron Radiation Facility for assistance with the XAS measurements, and the Shanghai Supercomputer Center for computational resources.

Keywords: cobalt · composite materials · counter electrode · dye-sensitized solar cells · graphene

How to cite: *Angew. Chem. Int. Ed.* **2016**, *55*, 6708–6712
Angew. Chem. **2016**, *128*, 6820–6824

[1] a) H. N. Tian, Z. Yu, A. Hagfeldt, L. Kloo, L. Sun, *J. Am. Chem. Soc.* **2011**, *133*, 9413; b) M. Grätzel, *Acc. Chem. Res.* **2009**, *42*, 1788.

[2] a) B. O'Regan, M. Grätzel, *Nature* **1991**, *353*, 737; b) A. Hagfeldt, G. Boschloo, L. C. Sun, L. Kloo, H. Pettersson, *Chem. Rev.* **2010**, *110*, 6595.

[3] M. J. Ju, J. C. Kim, H. J. Choi, I. T. Choi, S. G. Kim, K. Lim, J. Ko, J. J. Lee, I. Y. Jeon, J. B. Baek, H. K. Kim, *ACS Nano* **2013**, *7*, 5243.

[4] a) X. J. Zheng, J. Deng, N. Wang, D. H. Deng, W. H. Zhang, X. H. Bao, C. Li, *Angew. Chem. Int. Ed.* **2014**, *53*, 7023; *Angew. Chem.* **2014**, *126*, 7143; b) E. B. Bi, H. Chen, X. D. Yang, W. Q. Peng, M. Gratzel, L. Y. Han, *Energy Environ. Sci.* **2014**, *7*, 2637; c) F. Gong, H. Wang, X. Xu, G. Zhou, Z. S. Wang, *J. Am. Chem. Soc.* **2012**, *134*, 10953.

[5] a) Z. B. Yang, M. K. Liu, C. Zhang, W. W. Tjiu, T. X. Liu, H. S. Peng, *Angew. Chem. Int. Ed.* **2013**, *52*, 3996; *Angew. Chem.* **2013**, *125*, 4088; b) Y. Y. Duan, Q. W. Tang, J. Liu, B. L. He, L. M. Yu, *Angew. Chem. Int. Ed.* **2014**, *53*, 14569; *Angew. Chem.* **2014**, *126*, 14797; c) M. X. Wu, X. A. Lin, A. Hagfeldt, T. L. Ma, *Angew. Chem. Int. Ed.* **2011**, *50*, 3520; *Angew. Chem.* **2011**, *123*, 3582; d) M. X. Wu, X. Lin, Y. D. Wang, L. Wang, W. Guo, D. D. Qu, X. J. Peng, A. Hagfeldt, M. Grätzel, T. L. Ma, *J. Am. Chem. Soc.* **2012**, *134*, 3419; e) J. Y. Wu, Y. M. Xiao, Q. W. Tang, G. T. Yue, J. M. Lin, M. L. Huang, Y. F. Huang, L. Q. Fan, Z. Lan, S. Yin, T. Sato, *Adv. Mater.* **2012**, *24*, 1884; f) Y. M. Xiao, J. H. Wu, J. Y. Lin, G. T. Yue, J. M. Lin, M. L. Huang, Y. F. Huang, Z. Lan, L. Q. Fan, *J. Mater. Chem. A* **2013**, *1*, 13885; g) Y. M. Xiao, J. H. Wu, J. Y. Lin, S. Y. Tai, G. T. Yue, *J. Mater. Chem. A* **2013**, *1*, 1289.

[6] a) K. S. Novoselov, A. K. Geim, S. V. Morozov, D. Jiang, M. I. Katsnelson, I. V. Grigorieva, S. V. Dubonos, A. A. Firsov, *Nature* **2005**, *438*, 197; b) D. H. Deng, K. S. Noveselov, Q. Fu, N. F. Zheng, Z. Q. Tian, X. H. Bao, *Nat. Nanotechnol.* **2016**, *11*, 218.

[7] a) Y. H. Xue, J. Liu, H. Chen, R. G. Wang, D. Q. Li, J. Qu, L. M. Dai, *Angew. Chem. Int. Ed.* **2012**, *51*, 12124; *Angew. Chem.* **2012**, *124*, 12290; b) L. Kavan, J. H. Yum, M. K. Nazeeruddin, M. Grätzel, *ACS Nano* **2011**, *5*, 9171; c) Y. X. Xu, H. Bai, G. W. Lu, C. Li, G. Q. Shi, *J. Am. Chem. Soc.* **2008**, *130*, 5856.

[8] M. Lefèvre, E. Proietti, F. Jaouen, J. P. Dodelet, *Science* **2009**, *324*, 71.

[9] a) F. Calle-Vallejo, J. I. Martinez, J. Rossmeisl, *Phys. Chem. Chem. Phys.* **2011**, *13*, 15639; b) S. Kattel, G. F. Wang, *J. Phys. Chem. Lett.* **2014**, *5*, 452.

[10] D. H. Deng, X. Q. Chen, L. Yu, X. Wu, Q. F. Liu, Y. Liu, H. X. Yang, H. F. Tian, Y. F. Hu, X. J. Cui, H. B. Li, J. P. Xiao, T. Xu, J. Deng, F. Yang, P. N. Duchesne, P. Zhang, J. G. Zhou, L. T. Sun, J. Q. Li, X. L. Pan, X. H. Bao, *Sci. Adv.* **2015**, *1*, e1500462.

[11] A. Hauch, A. Georg, *Electrochim. Acta* **2001**, *46*, 3457.

[12] a) J. K. Nørskov, F. Abild-Pedersen, F. Studt, T. Bligaard, *Proc. Natl. Acad. Sci. USA* **2011**, *108*, 937; b) A. J. Medford, J. Wellendorff, A. Vojvodic, F. Studt, F. Abild-Pedersen, K. W. Jacobsen, T. Bligaard, J. K. Nørskov, *Science* **2014**, *345*, 197; c) J. K. Nørskov, T. Bligaard, J. Rossmeisl, C. H. Christensen, *Nat. Chem.* **2009**, *1*, 37; d) B. Hammer, J. K. Nørskov, *Adv. Catal.* **2000**, *45*, 71; e) J. K. Nørskov, T. Bligaard, B. Hvolbaek, F. Abild-Pedersen, I. Chorkendorff, C. H. Christensen, *Chem. Soc. Rev.* **2008**, *37*, 2163; f) A. Michaelides, Z. P. Liu, C. J. Zhang, A. Alavi, D. A. King, P. Hu, *J. Am. Chem. Soc.* **2003**, *125*, 3704; g) T. R. Munter, T. Bligaard, C. H. Christensen, J. K. Nørskov, *Phys. Chem. Chem. Phys.* **2008**, *10*, 5202.

[13] Y. Hou, D. Wang, X. H. Yang, W. Q. Fang, B. Zhang, H. F. Wang, G. Z. Lu, P. Hu, H. J. Zhao, H. G. Yang, *Nat. Commun.* **2013**, *4*, 1583.

Received: February 29, 2016
Published online: April 18, 2016

